PROCEEDINGS of the
23rd International Congress on Acoustics
9 to 13 September 2019 in Aachen, Germany

The suppressed sound of inhomogeneous flapping airfoils

Michael WEIDENFELD[(1)], Eran ARAD[(2)]

[(1)]RAFAEL, Israel, wmichael@rafael.co.il
[(2)]RAFAEL, Israel

Abstract

We study the aeroacoustic problem of a flapping airfoil in a high-Reynolds and low-Mach regime, and propose novel means to reduce the far-field sound originated by the fluid-structure interaction. The present model consists of a two-dimensional, elastic airfoil, periodically actuated at the leading edge. The near-field is analyzed using thin airfoil theory, and a discrete-vortex wake-model. The derived airfoil motion and wake dynamics are then introduced as a source term to Powell-Howe's acoustic analogy, to project the sound towards a distant observer. Considering the elastic flapping configuration, we seek optimal material properties and a linear thickness distribution to reduce the sound of an otherwise rigid airfoil while retaining the lift amplitude of the rigid configuration. To this end, the aeroacoustic model is introduced into an optimization scheme, yielding an effective Pareto front, reflecting the trade-off between the competing objectives of lower sound levels and aerodynamic efficiency. Compared with the rigid heaving airfoil, over 10 [dB] sound reduction was obtained for the optimal flexible configuration with linear thickness distributions, producing the same lift amplitude. The optimal configurations are obtained by time shifting the motion- and wake-dipoles to antiphase mode, thus mitigating the total radiated sound, while keeping the lift-amplitude value. The opposing sound dipoles follow from the synchronized disposition of the airfoils' motion and circulation signals.

Keywords: Vortex sound, Optimization, Airfoil noise, Flapping noise, Vibro-acoustics

Introduction

The canonical fluid-structure interaction problem involving a flapping flexible sheet (flag, airfoil, sail, etc.) immersed in a uniform flow, is analyzed in the present work in an attempt to study novel means to mitigate the associated far-field noise. In general, the unsteady filament motion, and the interaction between the surface and wake vorticity, give rise to acoustic pressure-waves which then radiate as sound (1). In line with the ongoing interest in controlling noise generated aerodynamically by airborne vehicles (2), for both civil and military applications, the study of far-field sound originating from unsteady surface motion, plays a key role.

The associated noise problem of flapping elastic sheets was recently studied in theoretical works which examined the sound radiation of rigid and flexible airfoils in unsteady motion and flow conditions (3, 4). Inspired by owls "silent flight" technology (5), incorporating non-uniform geometry and elastic properties as a methodology for noise reduction, Weidenfeld and Manela (6) studied the role of airoil's permeability in reducing flapping noise. Their results reveal the negating effect of the opposing seepage- and motion-dipoles, on the total sound radiation.

In the context of flapping-wings noise, variable geometry and mass distribution is often considered, and introduced into various optimization schemes (7, 8), where a Pareto front of best possible designs is sought. The objective of the present work is to investigate means to control and reduce the sound of a flapping elastic filament, with regards to the aerodynamic performance, by varying geometry and structural features along the chord. To this end, we consider a two-dimensional setup of a thin elastic airfoil, periodically actuated at the upstream leading-edge, and free at the downstream trailing-edge. The near-field description includes a discrete-wake model, and the far-field acoustics is obtained via Powell-Howe acoustic analogy (1), valid for low-Mach and high-Reynolds number flow regime as is considered in the present work. Considering this setup, an optimization problem is formulated and a Pareto-optimal solution is obtained.

Problem formulation

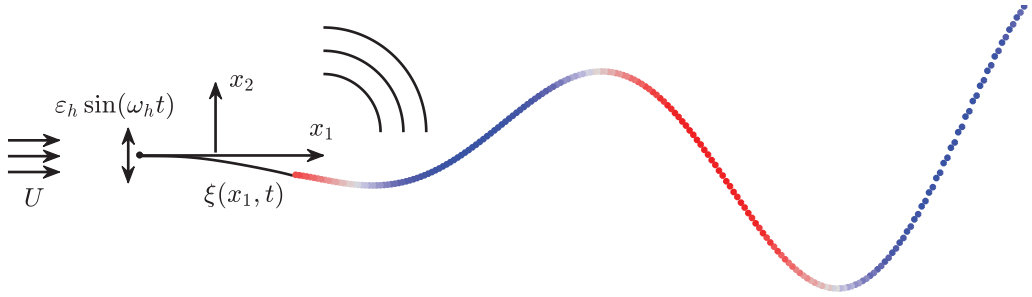

Figure 1. Problem schematics: An elastic airfoil immersed in a uniform flow and actuated at the leading edge by small amplitude heaving motion. The model includes trailing edge wake shedding in the form of discrete point vortices with negative (red) and positive (blue) circulations.

The problem schematics is shown in figure 1. An inextensible, thin flexible airfoil extending over the interval $-a \leq x_1 \leq a$ is immersed in a uniform flow of mean density ρ_0 with velocity U in the x_1-direction. The structure has a span L in the x_3-direction and thickness distribution $\sigma(x_1)$ with $\max(\sigma) \ll a \ll L$ such that the airfoil motion may be regarded two-dimensional in the x_1x_2-plane. At $t \geq 0$ leading-edge sinusoidal heaving actuation is applied,

$$\xi(x_1 = -a) = \overline{\varepsilon}_h a \sin(\omega_h t). \tag{1}$$

Here, $\xi(x_1,t)$ marks the filament displacement in the x_2 direction, $\overline{\varepsilon}_h \ll 1$ the scaled heaving amplitude (hereafter, overbars marks non-dimensional quantities), and ω_h denotes the heaving frequency. The displacement $\xi(x_1,t)$ is governed by the linear Euler-Bernoulli's beam equation

$$\rho_s(x_1)\frac{\partial^2 \xi}{\partial t^2} + \frac{\partial^2}{\partial x_1^2}\left(B(x_1)\frac{\partial^2 \xi}{\partial x_1^2}\right) = -\Delta p(x_1,t). \tag{2}$$

In (2), $\rho_s(x_1)$ and $B(x_1)$ mark the mass per unit area and bending rigidity chord-wise distributions, in units [kg/m^2] and [N·m], respectively. For a uniform structure in the x_3 direction, these properties are given by

$$\rho_s(x_1) = \rho_m \sigma(x_1), \tag{3}$$

$$B(x_1) = E\sigma^3(x_1)/12. \tag{4}$$

In (3)-(4), ρ_m is the material density, and E is Young's modulus. Assuming high Reynolds and low Mach conditions, and a small amplitude motion induced by the leading-edge heaving, the flow is regarded potential, and thin airfoil theory approximation is applied. At the small amplitude motion and induced angles of attack, the flow is considered attached throughout the airfoil and so vorticity is released continuously from the trailing edge. The present wake model consists of discrete line vortices, where at each time step $t = n\Delta t$, a new vortex is formed and placed adjacent to the instantaneous trailing edge position $(x_1,x_2) = (a+U\Delta t, \xi(a,t))$. The vortex strength Γ_k is fixed by Kelvin's theorem and the instantaneous airfoil circulation, and its trajectory follows from the potential flow computation.

Aeroacoustic scheme

The entire aeroacoustic problem is described in details by Weidenfeld et al. (9) and a short summary is given here, for brevity. As follows from thin airfoil theory, the airfoil is represented by its circulation distribution

along the chord $\gamma(x_1,t)$. Turning to complex notation, $z = x_1 + ix_2$ represents location on the complex z-plane and $W(z)$ marks the conjugate velocity flow field derived from the potential theory. The airfoil impermeability condition is then given by

$$\frac{\partial \xi}{\partial t} + U\frac{\partial \xi}{\partial x_1} = -\operatorname{Im}\{W(z)|_{-a\le x_1\le a}\}. \tag{5}$$

The pressure jump $\Delta p = p_+ - p_-$ across the airfoil, appearing on the right-hand side of (2), marks the fluid loading owing to the lower (p_-) and upper (p_+) surface pressure difference, and is related to the airfoil circulation $\gamma(x_1,t)$ via the unsteady Bernoulli's equation

$$\Delta p(x_1,t) = \rho_0 U\gamma(x_1,t) + \rho_0\frac{\partial}{\partial t}\int_{-a}^{x_1}\gamma(s,t)\,\mathrm{d}s. \tag{6}$$

Wake vortices dynamics is coupled to the system through the right-hand side of the impermeability condition (5). In addition, Kelvin's theorem is imposed

$$\Gamma_N = -\sum_{k=1}^{n-1}\Gamma_k - \int_{-a}^{a}\gamma(x_1,t)\,\mathrm{d}x_1, \tag{7}$$

ensuring the system total circulation vanishes at all times, and fixing the strength of the recently shed vortex Γ_N. To complete the formulation of the problem and set regular flow along the airfoil surface and finite velocity at the trailing edge, we apply the unsteady Kutta condition, fixing the vanishing trailing edge circulation. In line with the equation of motion (2), and free-end condition at $x_1 = a$, the well imposed problem consists of the four boundary condition

$$\xi(-a,t) = \overline{\varepsilon}_h a\sin(\omega_h t),\ \left(\frac{\partial \xi}{\partial x_1}\right)_{(-a,t)} = 0,\ \left(\frac{\partial^2 \xi}{\partial x_1^2}\right)_{(a,t)} = 0,\ \left(\frac{\partial^3 \xi}{\partial x_1^3}\right)_{(a,t)} = 0, \tag{8}$$

and accompanied by the homogeneous initial state of the airfoil at $t = 0$.

Having formulated the near-field problem, we now turn to the acoustic radiation scheme in which the former serves as an effective "source term" to be radiated to the far-field. In the present low-Mach and high-Reynolds flow regime, the acoustic pressure is governed by the linear inhomogeneous wave equation (1)

$$\left(\frac{1}{c_0^2}\frac{\partial^2}{\partial t^2} - \nabla^2\right)p = \rho_0\frac{\partial^2 \xi}{\partial t^2}\delta(f_a) + \rho_0\nabla\cdot(\Omega\times\mathbf{v}), \tag{9}$$

where c_0 marks the mean speed of sound, $\mathbf{v}$ is the fluid velocity, δ is the Dirac delta function and the function $f_a = f_a(\mathbf{x},t)$ vanishes on the airfoil surface. The vorticity field, denoted by Ω is given by the sum of all wake vortices circulation

$$\Omega = \hat{\mathbf{x}}_3\sum_{k=1}^{n}\Gamma_k\delta\left(\mathbf{x} - \mathbf{x}_{\Gamma_k}(t)\right). \tag{10}$$

In (10), $\mathbf{x}_{\Gamma_k}(t)$ marks the instantaneous k-th vortex location, and the hat denotes a unit vector. The *total* acoustic pressure is decomposed into the sum of *motion* (p_ξ) and *wake* (p_w) dipole contributions,

$$p_{\mathrm{tot}}(\mathbf{x},t) = p_\xi(\mathbf{x},t) + p_w(\mathbf{x},t), \tag{11}$$

where

$$p_\xi(\mathbf{x},t) = \frac{\rho_0\cos\theta}{2\pi\sqrt{2c_0|\mathbf{x}|}}\frac{\partial}{\partial t}\int_{-\infty}^{t_r}\frac{\mathrm{d}\tau}{\sqrt{t_r-\tau}}\int_{-a}^{a}\sqrt{a^2-y_1^2}\frac{\partial^2 \xi}{\partial \tau^2}(y_1,\tau)\,\mathrm{d}y_1, \tag{12}$$

$$p_w(\mathbf{x},t) = \sum_{k=1}^{n}\frac{\rho_0\Gamma_k}{2\pi\sqrt{2c_0|\mathbf{x}|}}\frac{\partial}{\partial t}\left(\sin\theta\int_{-\infty}^{t_r}\frac{V_{\Gamma_k}^{(2)}(\tau)\,\mathrm{d}\tau}{\sqrt{t_r-\tau}}\right.$$
$$\left. -\cos\theta\int_{-\infty}^{t_r}\frac{\mathrm{d}\tau}{\sqrt{t_r-\tau}}\left(V_{\Gamma_k}^{(1)}(\tau)\frac{\partial Y_2}{\partial y_2} - V_{\Gamma_k}^{(1)}(\tau)\frac{\partial Y_2}{\partial y_1}\right)_{\mathbf{x}_{\Gamma_k}(\tau)}\right). \tag{13}$$

In (12)-(13), $V_{\Gamma_k}^{(j)}$ marks the k-th vortex velocity component in the x_j-direction. The angle θ specifies the far-field observer's inclination, measured clockwise from the x_2-axis. Accordingly, the lift and suction dipoles are identified as the terms involving the $\cos\theta = x_2/|x|$, and $\sin\theta = x_1/|x|$, respectively.
We focus on acoustic wavelengths λ_0 far larger than the airfoil chord $\lambda_0 \gg a$, which equivalently specifies $\overline{\omega}_0 M \ll 1$, where $\overline{\omega}_0 = \omega_0 a/U$ is the reduced acoustic frequency. In line with the low Mach number working frame, this confines the analysis to low-moderate acoustic frequencies satisfying $\overline{\omega}_0 \ll 1/M$, and allowing the application of compact scheme using the two-dimensional compact Green's function (1), introduced into equations (12)-(13).
Before proceeding and for future reference we introduce the total acoustic lift dipole ($\theta = 0$)

$$p_{\text{tot}}^{\text{Lift}}(x_2,t) = p_{\text{tot}}(x_1 = 0, x_2, t) = p_\xi(x_1 = 0, x_2, t) + p_w(x_1 = 0, x_2, t) \tag{14}$$

Optimization scheme

Consider a rigid heaving airfoil, producing unsteady lift with amplitude $\|L\|_{\text{rigid}}$, and radiating sound to a distant observer in the x_2-direction with amplitude $\|p_{\text{tot}}\|_{\text{rigid}}$, where the norm sign $\|x\|$ denotes the *maximum* norm of the variable x, throughout the paper. We seek an alternate elastic, non-homogeneous airfoil, with optimal thickness distribution along the chord, to minimize the amplitude of the far-field acoustic lift dipole without compromising on the rigid airfoil's lift amplitude. Accordingly, The optimization problem is given by

$$\begin{aligned} \text{minimize} \quad & \|p_{\text{tot}}^{\text{Lift}}\|, && \text{(15a)} \\ \text{with respect to} \quad & \sigma(x_1), \rho_m, E, && \text{(15b)} \\ \text{subject to} \quad & \|L\| \geq \|L\|_{\text{rigid}}\,(\pm 33\%), && \text{(15c)} \end{aligned}$$

where the cost function is the lift dipole amplitude, the input variables are the airfoil thickness distribution, material density, and the Young modulus, and the minimization is subjected to a minimum lift amplitude constraint with a 33% tolerance for faster convergence and to obtain a sufficiently wide Pareto Front. The optimization process is executed using the modeFRONTIER® software (10), and involves a mixed-strategies practice, in which three methods are combined consecutively: the evolutionary MOGA-II (11), the heuristic Nelder & Mead Simplex (12), and the gradient based NLPQLP method (13). The genetic search is the process through which the a Pareto front materializes. The Simplex and gradient based search are then used to fine-tune a design around a specific constraint value.

Scaling and numerical procedure

The problem outlined hitherto, consists of the near- and far-field descriptions and the optimization framework. We now proceed and devise the non-dimensional form of the problem using a, U, a/U, $\rho_0 U^2$, and $2\pi a U$ as reference quantities for the length, velocity, time, pressure and vortices circulation, respectively. The non-dimensional quantities, marked by overbars, governing the aeroacoustic problem are

$$\overline{\rho} = \frac{\rho_m}{\rho_0}, \quad \overline{E} = \frac{E}{12\rho_0 U^2}, \quad \overline{\sigma}(\overline{x}_1) = \frac{\sigma(x_1)}{a}, \quad \overline{L}(\overline{t}) = \frac{L(\overline{t})}{\rho_0 U^2 a}, \tag{16}$$

denoting the material to air density ratio, normalized elasticity, thickness ratio, and the normalized lift force, respectively. Applying the same scaling to the acoustic problem (equations (12), (13), and (11)), the non-dimensional acoustic pressure takes the form

$$\overline{p}_{\text{tot}}(\overline{\mathbf{x}},t) = \sqrt{\frac{M}{8\,|\overline{\mathbf{x}}|}}\,\pi_{tot} = \sqrt{\frac{M}{8\,|\overline{\mathbf{x}}|}}\left(\pi_\xi(\overline{t}_r) + \pi_w(\overline{t}_r)\right), \tag{17}$$

where π_ξ, and π_w represent the acoustic *motion-* and *wake-* "kernels", respectively. In addition, the coupled dynamical-acoustic problem is further governed by

$$\overline{\varepsilon}_h, \overline{\omega}_h = \frac{a}{U}\omega_h, \theta = \arccos\left(\frac{\bar{x}_2}{|\overline{\mathbf{x}}|}\right) \tag{18}$$

marking the scaled heaving amplitude and angular frequency, and the observer far-field directivity, respectively. The scaled optimization problem is then specified by

$$\begin{aligned} \text{minimize} \quad & \|\pi_{\text{tot}}^{\text{Lift}}\|, && \text{(19a)} \\ \text{with respect to} \quad & \overline{\sigma}(\bar{x}_1), \overline{\rho}, \overline{E}, && \text{(19b)} \\ \text{subject to} \quad & \|\overline{L}\| \geq \|\overline{L}\|_{\text{rigid}}\,(\pm 33\%), && \text{(19c)} \end{aligned}$$

In all cases considered, the heaving amplitude and angular frequency were fixed by $\overline{\varepsilon}_h = 0.01$, and $\overline{\omega}_h = 1$ in accordance with the small amplitude motion and attached flow throughout the airfoil assumptions, set in Sec. 3. In the present setup, only combinations leading to the system's periodic state are considered. The numerical procedure requires discretization in both space and time. Thus the airfoil circulation distribution $\overline{\gamma}(\bar{x}_1, \bar{t})$ is decomposed into $N_\gamma = 100$ discrete vortices, and the time step is set to $\pi/65$, which proved sufficient for convergence. The system of equations was integrated using Euler's explicit method for 8 heaving cycles, unless divergence was detected first, originating from unstable parameters combination. We focus on linear thickness distribution of following form

$$\overline{\sigma}(\bar{x}_1) = \beta_1 \bar{x}_1 + \beta_0, \tag{20}$$

and begin by seeking first an optimal elastic structure whose thickness is uniform throughout the chord ($\beta_1 = 0$). We then move on to a structure whose thickness varies linearly along the chord.

Results

6.1 Uniform thickness distribution

In the present section we seek a heaving elastic filament with uniform thickness which produces the same lift amplitude as it's rigid counterpart and radiates lower sound levels to a far-field observer. All far-field results are given in the lift dipole direction and so the π^{Lift} superscript is omitted from all dipoles for brevity. Figure (2) presents a scatter map relating the sound reduction with respect to the rigid case (vertical axis), and the lift amplitude ratio (horizontal axis). The blue markers represent all *feasible* configurations (satisfying the lift amplitude constraints), and the red markers represent the discrete Pareto front. The horizontal dashed line marks zero sound reduction, and the vertical dashed line marks the rigid setup lift amplitude. The uniform thickness distribution results, identified by the square markers, indicate that no stable elastic configuration of uniform thickness produces lower sound levels without an aerodynamic compromise. A minor sound reduction of about ~ 2 [dB] is obtained for the substantial cost of a 33% in lift amplitude. We therefore proceed to examine variable thickness configurations, starting with a linear distribution.

6.2 Linear thickness distribution

By linearly varying the airfoil thickness along the chord, numerous configurations are found to both reduce sound levels and satisfy the lift amplitude constraint, as illustrated by the dot markers in figure (2). In figure (2), the red dot markers represent the actual discrete Pareto front obtained from the optimization process, and the solid curve is a suggested theoretical continuous front in the form of linear relation between the sound reduction and lift amplitude ratio. In the uniform thickness case, there was no indication for such linear relation. Additionally, the results illustrated in figure (2), visualize the differences between the two Pareto fronts, highlighting the radical improvement in sound reduction, simply by allowing the the airfoil thickness to vary linearly along the chord.

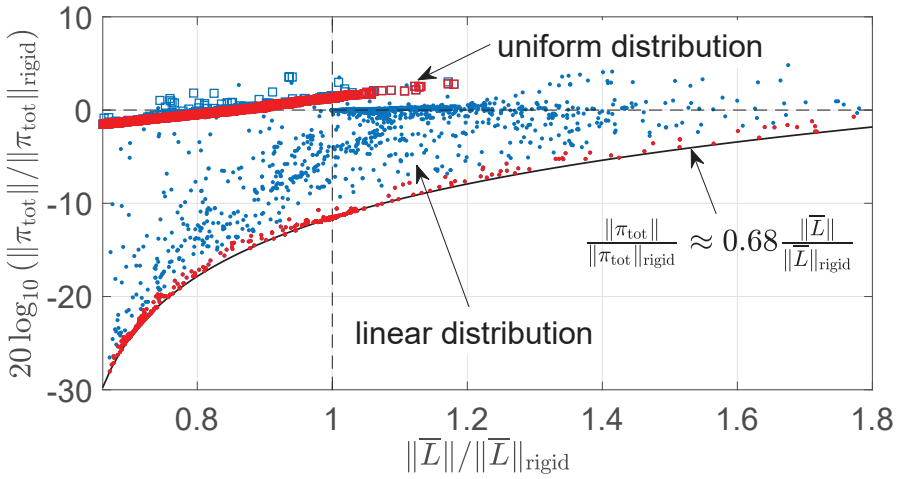

Figure 2. Scatter map of noise reduction (in [dB]) vs. lift ratio depicting *real* configurations (blue markers) and the discrete Pareto front (red markers). Square markers represent uniform thickness distribution results, dots represent linear thickness distribution results. The solid black line marks a theoretical Pareto front. The horizontal dashed line marks zero sound reduction, and the vertical dashed line marks the rigid setup lift amplitude. The dashed lines intersections mark the rigid configuration setup.

The optimal results are rationalized through the mechanism suggested in figures (3a)-(3c). All three figures present the motion and wake lift-dipole contributions, along with the total lift kernel, obtained for the rigid setup (3a), the optimal configuration satisfying $\|\overline{L}\| = \|\overline{L}\|_{\rm rigid}$ (3b), and the optimal configuration satisfying $\|\overline{L}\| = 0.67\|\overline{L}\|_{\rm rigid}$ (3c). The optimal configurations clearly present similar trends, in figures (3b)-(3c), which significantly differ from that of the rigid configuration in (3a). The results indicate that optimal configurations are obtained when two conditions are met:

1. The motion dipole is similar in magnitude to that of the rigid case,
2. The motion and wake dipoles are in antiphase.

The motion sound reflects the unsteady forces exerted on the fluid by the airfoil motion, consequently, keeping it's magnitude similar to that of the rigid case, maintains the lift constraint. In addition, setting the motion and wake dipoles in antiphase acts to mitigate the overall sound of the fluid-structure interaction.
Turning to the near-field dynamics, under the non-dimensional actuation frequency of $\overline{\omega}_h = 1$, all Pareto designs exhibit an airfoil motion resembling the first mode of a cantilever beam, as suggested by the deflection obtained for the $\|\overline{L}\| = \|\overline{L}\|_{\rm rigid}$ optimal results presented in figure (4a). Each point along the chord features a phase lag with respect to the leading edge motion. To represent the entire beam, we may define an average beam motion

$$\left\langle \overline{\xi} \right\rangle = \frac{1}{2}\int_{-1}^{1} \overline{\xi}(\bar{x}_1,\bar{t})\,\mathrm{d}\bar{x}_1. \tag{21}$$

Recalling Kelvin's theorem from eq. (7), the airfoil and wake circulations amount to zero, so that $\overline{\Gamma}_{\rm airfoil}(\bar{t}) = -\overline{\Gamma}_{\rm wake}(\bar{t})$. Figure (4b) compares between the average beam motion and both circulation time-variations over a period of motion for the $\|L\| = \|L\|_{\rm rigid}$ optimal design. The trends provide a complementary dynamical view of the optimal results, suggesting that synchronizing the airfoil motion and circulation is required for ultimately reducing far-field sound. It follows that the motion and wake-circulation are set to be in antiphase, which then promotes the counterpart antiphased sound-dipoles leading to the desired "silent" outcome. Figure (4c)

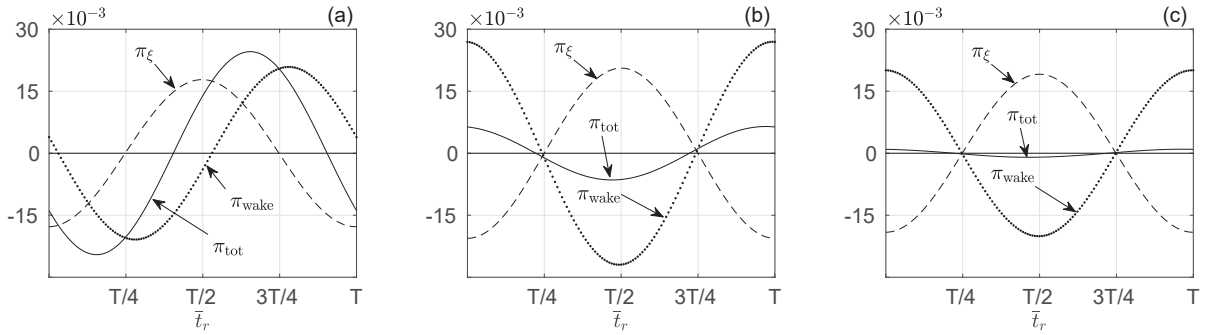

Figure 3. Sound components for three problem setups. (a) Rigid setup, (b) optimal configuration satisfying $\|\overline{L}\| = \|\overline{L}\|_{\text{rigid}}$, (c) optimal configuration satisfying $\|\overline{L}\| = 0.67\|\overline{L}\|_{\text{rigid}}$. Three different curves mark the motion dipole (- - -), wake dipole (·····), and total sound dipole (——).

presents the absolute phase-difference between average beam motion and wake-circulation (blue), and airfoil-circulation (red), for all Pareto optimal results. The results reinforce the previous observation and indicate that all Pareto results exhibit locked-in motion and airfoil-circulation signals, and antiphased motion and wake-circulation signals.

Examining the geometry features, the results indicate that all Pareto-optimal designs share a negative slope

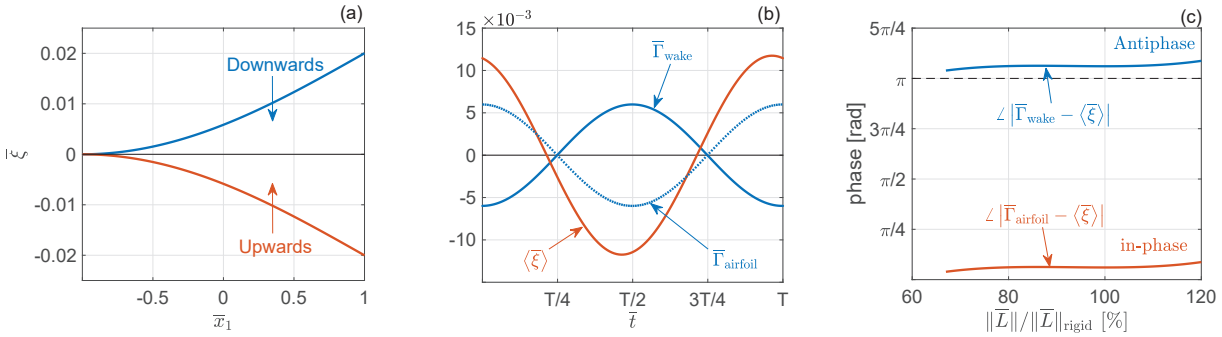

Figure 4. Near field dynamics. (a) Airfoil instantaneous deflection at $\overline{\xi}(-1,t) = 0$. The blue curve corresponds to a downward accelerating airfoil, and the red curve corresponds to upward acceleration. (b) The solid red curve represents the average airfoil motion $\left\langle\overline{\xi}\right\rangle$, the solid red curve represents the wake circulation, and the dotted red curve represents the airfoil circulation. Results are plotted over a motion period for the $\|L\| = \|L\|_{\text{rigid}}$ optimal design. (c) Blue curve marks the absolute phase-difference between average beam motion and wake-circulation, and the red curve marks the absolute phase-difference between average beam motion and airfoil-circulation. Both curves represent the Pareto-optimal results for linear thickness distribution and plotted for various lift-constraint values.

resulting with a thicker leading edge and a thinner trailing edge, where the higher-lift designs feature smaller slope values and the lower-lift designs are of slightly larger slopes.

Conclusion

In the present study we considered the effect of non-uniform thickness distribution on the sound radiation of an elastic, leading-edge actuated, two-dimensional thin airfoil, in a low-Mach potential uniform flow. Using thin

airfoil theory along with a discrete wake model, the near-field dynamics was obtained and introduced as an effective dipole-type source term to the Powell-Howe acoustic analogy, to obtain the far-field sound.
The aeroacoustic setup, was then introduced into an optimization scheme where optimal material properties and thickness distribution was sought. The objective was to minimize flapping sound with respect to a rigid heaving configuration while retaining the rigid setup lift-amplitude value. It was found that uniform flags inefficiently reduce sound in about $\sim$2 [dB], compared with the rigid airfoil, at the cost of 33% of the lift-amplitude.
In contrast, the optimal linear thickness configuration was found to reduce flapping sound in about $\sim$10 [dB] compared with the rigid setup, while retaining the same lift amplitude. The Pareto front was found to exhibit an approximated linear relation between sound reduction and lift-amplitude ratio, exhibiting a further substantial sound reduction of up to $\sim$30 [dB] for smaller lift amplitude values.
The mechanism through which sound reduction is obtained for a specific lift-amplitude value is two-fold: (1) The motion and wake dipoles are shifted to counteract each other and reduce the total sound emitted, (2) the motion dipole, reflecting the unsteady forces excreted on the fluid by the airfoil motion, is fixed in magnitude to the rigid setup value, thus maintaining the desired lift amplitude value. The antiphase merit between the two sound dipoles was found to follow from phase-locking the airfoil motion and circulation.

REFERENCES

1 Howe MS. Theory of Vortex Sound. Cambridge Texts in Applied Mathematics. Cambridge University Press; 2003.

2 Zaporozhets O, Tokarev V, Attenborough K. Aircraft Noise. New York: Taylor and Francis; 2011.

3 Manela A. Vibration and sound of an elastic wing actuated at its leading edge. Journal of Sound and Vibration. 2011;331:638–650. doi:10.1016/j.jsv.2011.09.020.

4 Manela A. On the acoustic radiation of a pitching airfoil. Physics of Fluids. 2013;25(7):071906. doi:10.1063/1.4816295.

5 Kroeger RA, Grushka HD, Helvey TC. Low speed aerodynamics for ultra-quiet flight. Tech Rep AFFDL-TR-71-75. 1972;doi:10.1016/0022-460X(71)90105-2.

6 Weidenfeld M, Manela A. On the attenuating effect of permeability on the low frequency sound of an airfoil. Journal of Sound and Vibration. 2016;375:275–288. doi:10.1016/j.jsv.2016.04.002.

7 Stanford BK, Beran PS. Analytical Sensitivity Analysis of an Unsteady Vortex-Lattice Method for Flapping-Wing Optimization. Journal of Aircraft. 2010;47(2):647–662. doi:10.2514/1.46259.

8 Stewart EC, Patil MJ, Canfield RA, Snyder RD. Aeroelastic Shape Optimization of a Flapping Wing. Journal of Aircraft. 2014;53(3):13–17. doi:10.2514/1.C033278.

9 Weidenfeld M, Arad E. Mitigating the sound of a flapping airfoil using optimal structural properties distributions. Journal of Sound and Vibration. 2018 oct;432:235–248. doi:10.1016/j.jsv.2018.06.016.

10 ESTECO. modeFRONTIER, [Software Package]; 2014.

11 Poles S. MOGA-II an improved multi-objective genetic algorithm. ESTECO - Technical Report. 2003;.

12 Poles S. The simplex method; 2003. 2003-005.

13 Schittkowski K. NLPQLP : A Fortran Implementation of a Sequential Quadratic Programming Algorithm with Distributed and Non-Monotone Line Search; 2010.